Improvement in sulfur desorption of NO_X storage and reduction catalysts using a Ba-Ti composite oxide.

Toshiyuki Tanaka [a]*, Ichirou Tajima [a], Yuichi Kato [a], Yasushi Nishihara [b], Hirofumi Shinjoh [a]

[a] *Toyota Central Research and Development Labs., Inc., Nagakute-cho, Aichi 480-11, Japan*

[b] *Division of Chemistry and Biochemistry, Graduate School of Natural Science and Technology, Okayama University, Tsushimanaka, Kita-ku, Okayama, 700-8530, Japan*

* Corresponding author. E-mail: e0924@mosk.tytlabs.co.jp, Tel: (+81-561)636140, fax: (+81-561)636150

Abstract

A Ba-Ti composite oxide was formed on a NOx storage and reduction catalyst via impregnation of a Ba-Ti precursor solution composed of H_2O_2 added to a complex prepared using the citric acid method. The structure of the Ba-Ti composite in solution was analyzed by chemical composition analysis and FT-Raman and UV-vis spectroscopy. MM2 calculations were performed to propose its chemical structure. Both Ba and Ti together were found to form a composite molecule in the solution. Furthermore, TEM-EDX and XRD analyses of the Ba-Ti composite oxide on the catalyst prepared by impregnation with the Ba-Ti composite aqueous solution revealed that Ba and Ti in the catalyst were highly dispersed at the nm scale. The formation of the Ba-Ti composite oxide on the NSR catalyst enhanced sulfur desorption efficiency and led to high-performance NO_X conversion as a NO_X storage and reduction activity catalyst after desulfation treatment. It was assumed that the existence of microscopic Ba compounds combined with Ti was efficient for the inhibition of the sintering of barium sulfate and its facile

decomposition. It was found that dispersion of Ba compounds for NO_X storage materials using a Ba-Ti complex solution is an efficient way to improve the durability of NSR catalysts.

Keywords: NSR catalyst, desulfation, Barium sulfate, Titanium oxide, citric acid

1. Introduction

Curbing CO_2 emissions and improving the fuel efficiency and clean-up of automobile exhaust gases are required for global environmental protection. Lean-burning gasoline and diesel engines achieve high fuel economy using higher air/fuel ratios (A/F). It is difficult, however, to remove the NO_X in exhaust gases from these engines under excess oxygen conditions. Some NO_X purifying systems such as selective NO_X reduction by hydrocarbons [1, 2, 3], NH_3 (urea) [4], H_2 [5] and CO [6] have been researched, with a few of them developed for commercial use.

A NO_X storage and reduction (NSR) catalyst system is one of the most efficient ways to achieve NO_X purification [7, 8]. In the NSR system, NO_X (NO) is oxidized to NO_2 over precious metals in the catalyst, then combined with NO_X storage materials and finally stored as nitrate ions. In the following reduction stage, under a stoichiometric or reductive atmosphere (rich), the stored nitrate ions are released as NO_X (NO or NO_2) from the NO_X storage materials and then reduced to nitrogen. The NSR catalyst system has the advantages of high performance and feasibility for purifying NO_X compared with other methods.

Unfortunately, NSR catalysts deactivate due to sulfur poisoning and/or thermal deterioration. Sulfur deactivation in particular is the most important problem to be solved. The sulfur poisons the precious metals [9, 10], supports [11] and NO_X storage materials [8, 9]. Furthermore, sulfur poisoning strongly influences the NO_X storage ability of the system. NSR

catalysts include some alkali metals or alkali earth metals that produce stable sulfates (SO_X) when exposed to exhaust gases. It has been confirmed that the adsorbed sulfur transforms the NO_X storage materials into sulfates [8, 9, 10]. The formation of nitrate on the storage compound is inhibited and thus the NO_X storage ability deteriorates. Consequently, the deactivation of NSR catalysts depends on the amount of sulfur poisoning of the catalyst [12]. Sulfur deactivation also depends on the particle size of the sulfate produced by the NSR catalyst [13]. It has been reported that the decomposition temperature of sulfates decreases if the $BaSO_4$ particles in the catalyst are kept under 3 nm in size [14].

There have been several reports about improving the sulfur tolerance of NSR catalysts based on the above research. One of the methods involved the usage of TiO_2 [15]. The decomposition temperature of sulfates on a TiO_2 support was found to be lower than that on an Al_2O_3 support under reducing conditions. By blending TiO_2 with Al_2O_3 [16], sulfur deposition was simultaneously suppressed and enhanced the NO_X storage of the sulfur-aged catalyst. The tolerance of the NSR catalyst against sulfur poisoning was successfully improved by the use of fine TiO_2 particles [17, 18, 19, 20]. The decomposition temperature of titanium sulfate is 150˚C, and is considerably lower than that of aluminum sulfate (770˚C) and cerium sulfate (900˚C) which are often used as supports. Accordingly, titanium sulfate that forms under exhaust gases including SO_X is assumed to be decomposed easily and release SO_X more readily compared with other oxides.

In conventional NSR catalysts, some alkali materials such as Ba and K compounds are supported on porous oxide supports such as Al_2O_3. The co-existence of both Ba and K is effective for expanding the active temperature range. The NO_X storage amount for the K containing NSR catalyst is higher than that of the Ba containing catalyst at high temperatures (over 450˚C and lower at low temperatures (under 450˚C). For this reason, both Ba and K are used [29]. While the utilization of Ba compounds

for the NSR catalyst is very important for NO_X storage performance, it also inhibits sulfur deterioration. Ba sulfate is more stable than other alkali sulfates [16], and thus more sulfur residue exists after desorption treatment on the Ba compounds in an NSR catalyst compared to the K compounds. Accordingly, desulfation of Ba containing NSR catalysts is the most important subject to address in order to prepare highly durable NSR catalyst systems.

Based on the above information, we felt that the most effective way to realize improvement of sulfur desorption from NSR catalysts would be to make highly homogeneous fine particles of Ba and Ti compounds on a high surface area support such as Al_2O_3. One of the most simple and effective methods for achieving this aim is to disperse a composite aqueous complex solution including both Ba and Ti on the high surface area support. Citrate complexation is an efficient precursor method for producing fine and homogenous Ba-Ti composite oxides such as perovskite type $BaTiO_3$ [21, 22, 23]. In this method, however, the complex in solution tends to polymerize and produce a precipitate, which makes it difficult to use for impregnation on support oxides. However, we found that the addition of H_2O_2 is effective for keeping the solution stable [24]. In this study, we prepared NSR catalysts using a Ba-Ti composite oxide dispersed on the support surface and examined their structures and catalytic performance.

2. Experimental

2.1 Catalyst preparation

2.1.1 Preparation of Ba-Ti composite solution

The preparation method is described as follows. Citric acid was first dissolved in water at 75˚C followed by addition of $Ti(i\text{-}PrO)_4$ (Wako Co.) with continuous stirring. After stirring at 75˚C for 5 h, the solution transformed to a light

yellowish transparent state without any precipitates. The solution was then cooled at room temperature and 30% aqueous H_2O_2 solution (Wako Co.) was added, resulting in a change of color from light yellow to red. Finally, aqueous $Ba(CH_3COO)_2$ (Wako Co.) was added to the transparent red solution to obtain the Ba-Ti composite solution as the precursor of the Ba-Ti composite adsorbent. We found that addition of H_2O_2 inhibited precipitation, making the Ba-Ti precursor solution more stable than when no additives were used. The prepared composite solution was suitable for impregnation on various oxide supports.

2.1.2 Catalyst preparation

Four catalyst formulations, BaTi-A, BaTi-B, Ba-A and Ba-B, as summarized in Table 1, were prepared in this study. Cordierite substrates (cylindrical, φ = 30 mm, L =50 mm, 400 cells per square inch) were first coated with two types of metal oxides; 1) 7 g γ–Al_2O_3 for characterization and 2)9.45 g mixed oxides including γ-Al_2O_3, ZrO_2 and TiO_2 for estimation of catalytic activity. The wash coat was deposited by first immersing the substrate in an aqueous slurry of the above oxides. The excess slurry was gently removed by blowing air through the monolith channels. The samples were then dried and subsequently calcined. The coating procedure was repeated until the desired amount of alumina was deposited and the samples were then calcined for 1 h at 500˚C in air. Catalysts were prepared by impregnating $Pt(NH_3)_2(NO_2)_2$ and $Rh(NO_3)_3$ (Tanaka Precious Metals) followed by drying at 110˚C for 12 h and then calcining at 300˚C for 3 h in air. The amount of Pt and Rh loading was 2 and 0.5 g/L, respectively. The monolith obtained was then added to an aqueous solution containing Ba_to form the storage material. The BaTi-A and BaTi-B catalysts were prepared using the Ba-Ti composite solution prepared above. The Ba-A and Ba-B catalysts were prepared using $(CH_3COO)_2Ba$. Finally, an aqueous solution containing CH_3COOK and CH_3COOLi (Wako Pure Chemical

Industries) was impregnated on the monolithic samples containing Pt and Rh, such as BaTi-B and Ba-B. The loading amounts of Ba, K and Li were 0.2, 0.15 and 0.1 mol/L, respectively. After the catalysts were dried at 110 ˚C for 12 h, they were calcined at 300˚C for 3 h in air.

2.2. Characterization of the Ba-Ti composite precursor solution

The structure of the Ba-Ti composite in solution was analyzed by chemical composition analysis and FT-Raman and UV-vis spectroscopy. Chemical composition analysis was performed on the solid obtained by accumulating the orange colored fraction separated by silica gel column chromatography using water as a solvent. The content of Ba and Ti were analyzed by ICP (SSI Nano-TEC SPS4000) and the content of C was analyzed by the combustion infrared absorption method (Horiba Co. EMIA810). The chemical structure of the Ba-Ti composite in solution was proposed by performing an optimized geometry calculation in mechanics using CAChe and SCiGRESS software (FUJITSU Limited) with augmented MM2 parameters based on the results of the above analyses.

2.3. Characterization of the catalysts

XRD patterns were recorded using an X-ray diffractometer (Cu Ka radiation l = 1.5418 Å, 40 kV, 30 mA) (Rigaku, RINT-1500V). Samples of catalyst powders were pressed into wafers and affixed to standard sized microscope slides. The particle size of Pt was calculated using Scherrer's formula.

The ratio of Ti to Ba in the BaTi catalyst powder was analyzed using an energy-dispersive X-ray (EDX) analyzer equipped with a field-emission transmission electron microscope (Hitachi, HF-2000). The diameter of the EDX analysis area was approximately 10 nm.

2.4. Thermal aging test and sulfur treatment

Thermal aging was performed by exposing the catalysts to 1 L/min of air at 750˚C for 5 h. Table 2 shows the composition of the feed streams used to simulate actual engine exhaust gases for the catalytic performance test using a conventional fixed-bed flow reactor (Best Sokki Bex-5900 with a flame photometric detector) at atmospheric pressure and fixed temperature. For the sulfur exposure treatment, catalysts were exposed to the SO_X adsorption gas atmosphere (Table 2), cycling lean (120 sec) and rich (3 sec) for 41 min at 400˚C. The total sulfur amount introduced to the catalyst during this treatment was 1.52 g/L-catalyst (47.6 mmol/L-catalyst), which was enough for sulfur deterioration of the NSR catalyst (vide infra). After the SO_X adsorption procedure, the gas composition was switched to the SO_X desorption atmosphere to measure the sulfur species desorbed from the catalysts. The gas hourly space velocity (GHSV) was 54,000 h^{-1} for both the adsorption and desorption steps.

2.5. Catalytic performance test

To investigate the influence of Ba-Ti composite oxides on the desulfation of the NSR catalysts, the deactivated catalysts were reduced under the sulfur desorption gas indicated in Table 2 at 600 or 650˚C for 10 min and subsequently exposed to sulfur-free lean–rich NO_X cycles as described above. These procedures were repeated several times. From the measured NO_X concentration, the NO_X conversion and NO_X storage amount were calculated.

3. Results and discussion

3.1. Structure of the Ba-Ti precursor

UV-vis, NMR and Raman spectra, chemical analysis and MD calculations were performed in order to propose a structure for

the Ba-Ti precursor.

UV-vis spectra of the Ba-Ti precursor solution are shown in Fig. 1. A peak around 380 nm is attributed to a Ti-peroxo complex [25,26], which indicates production of O_2 following addition of H_2O_2 and then coordination of O_2 to Ti.

The chemical composition of the red-orange part of the solution, separated by using silica gel column chromatography, is presented in Table 3. Both Ba and Ti were included in the separated solution, and the ratio of Ba to Ti was 0.7 to 1.0. This result suggests that there is a high possibility of Ba and Ti-O_2 complexes coexisting in the same molecule.

Raman spectra of the Ba-Ti solution and the ingredients used to prepare it are depicted in Fig. 2. Some characteristic peaks were noted. A peak around 620 cm^{-1} was detected in the Ba-Ti precursor solution (a) and the solution of Ti citric acid and H_2O_2 (b) but not in the Ti citric acid solution (c), H_2O_2 solution (d) or the $Ba(CH_3COO)_2$ solution (e). The peak was attributed to a Ti-(O_2) bond as reported by Fang [27]. A 900 cm^{-1} peak was also detected in both solutions containing Ti, citric acid and H_2O_2 (a and b). It was attributed to an O-O bond of the Ti-O_2 complex as previously reported [27]. A 370 cm^{-1} peak was detected only for the Ba-Ti precursor solution. We confirmed that this peak increased with increasing concentration of Ba acetate solution and reached a maximum when Ba/Ti= 1. Based on a previous identification by Su [28], we think this peak results from a Ba-O bond in the Ba-Ti precursor solution.

The XRD patterns of the powders obtained after calcining the precursors in air at 650˚C for 3 h are shown in Fig. 3. XRD patterns of the calcined powders showed that the crystallization of the precursor occurred at 650˚C and only $BaTiO_3$ perovskite was formed without the presence of other crystalline phases such as $BaCO_3$ and TiO_2. This result means that Ba and Ti exist in a state resulting from their facile combination in the precursor solution.

MM2 calculations were performed based on the results obtained for the chemical analysis and from the UV-vis and Raman

spectra. Firstly, based on Fang's previous report [27], a stabilized cage type structure containing Ba^{2+}, Ti^{4+} and 6 molecules of citric acid was calculated. It was found, however, that one molecule of coordinated citric acid is comparatively unstable and easily displaced by a peroxo ligand in the presence of H_2O_2, forming a more stabilized structure. This estimated stable structure of the complex in the Ba-Ti precursor solution prepared above is shown in Fig. 4. The cage type structure with Ba and Ti surrounded by 5 citric acid molecules can be clearly seen. The improved stability of this prepared Ba-Ti composite structure is likely the reason that this form is preferred.

The analysis of the data described above about the Ba-Ti composite solution supports the idea that both Ba and Ti together form a composite molecule in the solution.

3.2. Structure of the Ba-Ti composite oxide with Pt on the support surface

XRD patterns of the BaTi-A and Ba-A catalysts after 500˚C calcination are shown in Fig. 5. A diffraction peak at 23.8˚, attributed to $BaCO_3$, was recognized for the Ba-A catalyst but not for the BaTi-A catalyst. No other peaks derived from Ba compounds such $BaCO_3$ and $BaTiO_3$ were detected for BaTi-A. This result suggests that the Ba compounds on the BaTi-A catalyst are well dispersed with a fine structure. It is assumed that the bulky caged structure of the Ba-Ti complex speculated above inhibits aggregation of Ba compounds on the calcined catalyst because of the formation of a composite oxide with Ti.

A TEM image of the BaTi-A catalyst is shown in Fig. 6. Ba and Ti were well dispersed on Al_2O_3 primary particles. No discrete particles such as $BaCO_3$, $BaTiO_3$ or TiO_2 were observed in the BaTi-A catalyst. This result indicates that Ba and Ti are present homogeneously on Al_2O_3. In order to clarify the Ba and Ti concentration on the Al_2O_3 particles, random analysis spots of Al_2O_3 primary particles were examined using EDX. The compositions of two selected spots are listed in Table 4. Ba

and Ti were detected in each analysis spot on the nm scale. Therefore, the surface of the Al_2O_3 particle was modified with Ba and Ti in a highly dispersed state, and this surface localization is expected to work effectively for sulfur resistance as discussed below.

The XRD patterns of the BaTi-B and the Ba-B catalysts after the sulfur exposure treatment are shown in Fig. 7. A diffraction peak at 43°, attributed to $BaSO_4$, was recognized on the Ba-B catalyst but not on BaTi-B. The size of the $BaSO_4$ particles on Ba-B was estimated using Scherrer's formula to be 10 nm. Because no sulfur concentration in the outlet gases from both of these catalysts during the sulfur exposure treatment was detected, the estimated amount of sulfur deposited on both of the catalysts was determined to be about 1.5 g/L (47 mmol/L). The comparison of the $BaSO_4$ peaks suggested that barium sulfate on BaTi-B was dispersed with a considerably fine structure compared with that on Ba-B. On the other hand, a diffraction peak at 39.8° attributed to Pt was recognized for both BaTi-B and Ba-B. The particle sizes of the Pt on the BaTi-B and Ba-B catalysts calculated from these diffraction peaks were 34 nm and 35 nm, respectively. It was found that this minor difference in Pt particle sizes did not affect the performance of the storage materials. Furthermore, the number of Pt active sites was equal in both catalysts. These results suggest that the addition of Ba compounds should have a predominant influence on the state of the NO_X storage materials and their catalytic performance.

The analysis of the supported BaTi catalysts revealed that utilization of the Ba-Ti composite solution led to formation of highly dispersed Ba compounds. Surface species on NSR catalysts composed of Ba (such as $BaCO_3$) have been reported to store NO_X and be converted to $BaSO_4$ through sulfur exposure [8]. Though no detailed information about the structure of the Ba compounds on our BaTi catalyst was gathered, it was assumed that the formation of fine structures of Ba compounds on the BaTi catalyst prevented the formation of crystalline $BaSO_4$.

3.3. Catalytic performance

Sulfur desorption profiles during rich treatment of the BaTi-B and Ba-B catalysts at 600˚C or 650˚C after the sulfur exposure treatment are depicted in Fig. 8. Further, the desorbed sulfur amount and the ratio of that amount to the inlet quantity during the sulfur desorption treatment are indicated in Table 5. The amount of desorbed sulfur from BaTi-B was higher than for the Ba-B catalyst at the same inlet gas temperature (more than 1.7 times). In these catalysts, Ba, K, and Li compounds are included as NO_X storage materials.

NO_X conversion activity on the BaTi-B and Ba-B catalysts was measured during the repetitive procedure consisting of sulfur adsorption and desorption treatment. The NO_X profiles during lean/rich cycling of the NSR catalysts at 400˚C after sulfur desorption at 600 or 650˚C are shown in Fig. 9. The NO_X storage amount for BaTi-B was higher compared to that for Ba-B. The transition of NO_X conversion at 400˚C during repetitive sulfur adsorption (lean/rich cycles for 20 times at 400˚C) and desorption (rich at 650˚C) for 3 cycles can be seen in Fig. 10. During the sulfur adsorption procedure, NO_X conversion gradually declined after 20 lean/rich cycles. After desulfation treatment, NO_X conversion recovered to the same level as the previous treatment, which indicated that sulfur poisoned the active site for NO_X storage.

The relationship between the amount of desorbed sulfur during desulfation treatment and the average amount of stored NO_X calculated from the concentration of NO_X during lean/rich cycles after sulfur desorption treatment at the different desorption temperatures on both the BaTi-B and Ba-B catalysts is shown in Fig. 11. The differences in NO_X storage activities between the tested catalysts during lean/rich cycles was similar to the differences in their sulfur desorption abilities.

On an NSR catalyst, NO_X is firstly stored during lean

conditions and then is reduced by reacting with reductants such as H_2 and CO during rich conditions (vide supra). The NSR reaction proceeds continuously through these repetitive processes. The important factors for performance of the catalyst are the dispersion of the platinum group metals and the storage materials, which take on the red-ox function, and the formation of nitrate by the reaction of NO_X. However, in this study of BaTi-B and Ba-B catalysts, the dispersion of Ba compounds as storage materials seems to be directly related to their performances because the particle size of Pt in both of the catalysts was nearly equal.

As previously noted, one of the most important problems to be solved with NSR catalysts is the deactivation by sulfur poisoning. The improvement of catalyst activity for rapid desulfation is also necessary to obtain high catalytic performance. The deterioration of the NO_X storage ability of the NSR catalyst corresponds to the amount of adsorbed sulfur on the surface, and the regeneration of the catalytic activity depends on its sulfur removal ability. For practical use of NSR catalysts, NO_X storage sites need to be recovered by desulfation in a very short time. Ba compounds play an important role in securing larger NO_X storage amounts but Ba sulfates are difficult to decompose. Sulfur desorption from Ba compounds strongly influences sulfur desorption from NSR catalysts. On the BaTi catalyst, we deduced that the formation of the fine Ba-Ti composite oxide identified from XRD and TEM analyses contributes to its high performance in sulfur desorption and is a primary factor for the high sulfur desorption ability.

On the BaTi-B catalyst, it is thought that the Ba compounds, by combining with Ti, are highly dispersed. Sintering of the sulfate during sulfur circulation is controlled in such a form, and this control leads to improvement in sulfur desorption. It has been shown that the decomposition temperature is lowered when the particle size of generated sulfates is smaller [13], and it has also been reported that barium sulfate with a particle size of 3 nm or less is resolved easily at lower temperature

[14]. Furthermore, using pore size controlled supports has been found to improve the decomposition of sulfates by physically inhibiting the sintering of the sulfate [30]. In addition to the improvement resulting from greater Ba dispersion, the combination with TiO_2 works advantageously for desorption of sulfur compounds because of the instability of Ti sulfate.

For practical use in a lean-burning exhaust, engine combustion management at a high temperature and rich atmosphere is necessary for reproducible sulfur deactivation with conventional NSR catalysts, which leads to a fuel penalty. Application of the Ba-Ti composite oxide for preparation of NSR catalysts makes it possible to shorten the treatment time for sulfur desorption because of its high sulfur desorption rate, resulting in improved catalyst performance with sulfur containing fuel.

4. Conclusions

We prepared a Ba-Ti composite aqueous solution using citric acid and H_2O_2 and then prepared an NSR catalyst containing a Ba-Ti composite oxide using this solution. It was found that by impregnation with the Ba-Ti composite aqueous solution, Ba and Ti in the catalyst were highly dispersed on the oxide support within the nm order size. Furthermore, the formation of the Ba-Ti composite oxide on the NSR catalyst enhanced sulfur desorption efficiency and led to high-performance NO_X conversion as a NO_X storage and reduction activity catalyst after desulfation treatment. It was assumed that the existence of microscopic Ba compounds combined with Ti was efficient for the inhibition of the sintering of barium sulfate and its facile decomposition. We believe that the dispersion of Ba compounds for NO_X storage materials using a Ba-Ti complex solution is an efficient way to improve the durability of NSR catalysts.

References

[1] M. Iwamoto, H. Yahiro, Y. Yu-u, S. Shundo, N. Mizuno, Shokubai (Catalyst) 32 (1990) 430.
[2] T. Tanaka, T. Okuhara, M. Misono, Appl. Catal. B 4 (1994)L1
[3] T. Tanaka, K. Yokota, N. Isomura, H. Doi, M. Sugiura, Appl. Catal. B 16 (1998) 199.
[4] F. Nakajima, I. Hamada, Catal. Today 29 (1996) 109; R.M. Heck, Catal. Today 53 (1999) 519.
[5] Japanese Patent No.3382361.
[6] Japanese Unexamined Patent Application Publication No. Hei 8-10575.
[7] N. Miyoshi, S. Matsumoto, K. Katoh, T. Tanaka, J. Harada, N. Takahashi, K. Yokota, M. Sugiura, K. Kasahara, SAE Tech. Paper 950809 (1995).
[8] N. Takahashi, H. Shinjoh, T. Iijima, T. Suzuki, K. Yamazaki, K. Yokota, H. Suzuki, N. Miyoshi, S. Matsumoto, T. Tanizawa, T. Tanaka, S. Tateishi, K.Kasahara, Catal. Today 27 (1996) 63.
[9] A. Amberntsson, B. Westerberg, P. Engstro¨m, E. Fridell, M. Skoglundh, Stud. Surf. Sci. Catal.; Catal. Deact. 1999 (1999) 317.
[10] E. Fridell, H. Persson, L. Olsson, B. Westerberg, A. Amberntsson, M. Skoglundh, Top. Catal. 16/17 (2001) 133.
[11] S. Matsumoto, Y. Ikeda, H. Suzuki, M. Ogai, N. Miyoshi, Appl. Catal. B 25 (2000) 115.
[12] P. Engström, A. Amberntsson, M. Skoglundh, E. Fridell, G. Smedler, Appl. Catal. B 22 (1999) L241.
[13] D. H. Kim, J. Szanyi, J. H. Kwak, T. Szailer, J. Hanson, C. M. Wang, C.H. F. Peden, J. Phys. Chem. B 110 (2006) 10441.
[14] X. Wei, X. Liu, M. Deeba, Appl. Catal. B 58 (2005) 41.
[15] H. Suzuki, R. Muramoto, N. Takahashi, Toyota Tech. Rev. 46 (1996) 68.
[16] S. Matsumoto, Y. Ikeda, H. Suzuki, M. Ogai, N. Miyoshi, Appl. Catal. B 25 (2000) 115.
[17] I. Hachisuka, H. Hirata, Y. Ikeda, S. Matsumoto, SAE Tech. Paper 2000-01-1196 (2000).
[18] H. Hirata, I. Hachisuka, Y. Ikeda, S. Tsuji, S. Matsumoto,

Top. Catal. 16/17 (2001) 145.
[19] N Takahashi, A. Suda, I. Hachisuka, M. Sugiura, H. Sobukawa, H, Shinjoh, Appl. Catal. B 72 (2007) 187.
[20] H. Imagawa, T. Tanaka, N. Takahashi, S. Matsunaga, A. Suda, H. Shinjoh, J. Catal. 251 (2007) 315.
[21] M. Rajendran, M. S. Rao, J. Solid State Chem. 113 (1994) 239.
[22] J-d. Tsay, T.t. Fang, J. Am. Ceram. Soc. 82 (1999) 1409.
[23] M. Kakihana, M. Arima, Chem. Mater. 11 (1999) 438.
[24] Japanese Unexamined Patent Application Publication No.2005-60147.
[25] F. Bonino, A. Damin, G. Ricchiardi, M. Ricci, G. Spano`, R. D'Aloisio, A. Zecchina, C. Lamberti, C. Prestipino, and S. Bordiga, J. Phys. Chem. B 108 (2004) 3573.
[26] D. Srinivas, P. Manikandan, S.C. Laha, R. Kumar, P. Ratnasamy, J. Catal. 217 (2003) 160.
[27] Fang, T.-T.; Wu, M.-S.; Tsai, J.-D. J. Am. Ceram. Soc. 85 (2002) 2984.
[28] H. B. Su, D. O. Welch, W. Wong-Ng, L. P. Cook, Z. Yang, Appl. Phys. LET. 91 (2007) 172510.
[29] I. Hachisuka, T. Yoshida, H. Ueno, N. Takahashi, A. Suda, M. Sugiura, SAE Tech. Paper 2002-01-0732 (2002).
[30] Japanese Unexamined Patent Application Publication No. 2002-11347.

Figure captions

Table 1
Catalyst formulations.

Table 2
Simulated gas compositions for the catalytic performance tests.

Table 3
Composition of the solid after column separation.

Table 4
Ba/Ti composition on Al_2O_3 primary particles observed by EDX analysis.

Table 5
Amount and ratio to inlet sulfur of desorbed sulfur during sulfur desorption.

Fig. 1. UV-vis spectra of Ba-Ti precursor solutions.

Fig. 2. Raman Spectra of the precursor solutions: a) Ba-Ti precursor solution ($Ba(CH_3COO)_2$ + Ti citric acid + H_2O_2), b) Ti citric acid + H_2O_2, c) $Ba(CH_3COO)_2$, d) H_2O_2 and e) $Ba(CH_3COO)_2$.

Fig. 3. XRD patterns of Ba-Ti composite oxides obtained after calcination of the precursor solutions at 650˚C for 5 h.

Fig. 4. Estimated structure of the Ba-Ti precursor complex.

Fig. 5. XRD patterns of fresh catalysts; a) BaTi-A and b) Ba-A.

Fig. 6. FE-TEM micrograph of the BaTi-A catalyst.

Fig. 7. XRD patterns of catalysts after sulfur aging: a) BaTi-B and b) Ba-B.

Fig. 8. Sulfur desorption profiles during SO_X regeneration from NSR catalysts: a) BaTi-B at 650˚C, b) BaTi-B at 600˚C, c) Ba-B at 650˚C and d) Ba-B at 600˚C.

Fig. 9. NO_X concentration profiles at 400˚C during lean/rich cycle test over BaTi-B and Ba-B after the sulfur desorption procedure at 600 and 650˚C.

Fig. 10. NO_X conversion change at 400˚C during repetitive sulfur adsorption procedures (20 lean/rich cycles at 400˚C) and desorption (rich at 650˚C) over a) BaTi-B and b) Ba-B catalysts.

Fig. 11. Relationship between desorbed sulfur and NO_X storage amounts after sulfur regeneration at 600˚C or 650˚C: a) BaTi-B at 650˚C, b) BaTi-B at 600˚C, c) Ba-B at 650˚C and d) Ba-B at 600˚C.

Table 1
Catalyst formulations

Catalyst	Support	Pt g/L	Rh g/L	Ba mol/L	Ti mol/L	K mol/L	Li mol/L
BaTi-A	γ-Al_2O_3	2	-	0.2	0.2	-	-
BaTi-B	mixed oxides	2	0.5	0.2	0.2	0.15	0.1
Ba-A	γ-Al_2O_3	2	-	0.2	-	-	-
Ba-B	mixed oxides	2	0.5	0.2	0.2	0.15	0.1

Table 2
Simulated gases composition for the catalytic performance tests

Atmosphere	O_2 %	NO ppm	CO %	H_2 %	THC ppmC	CO_2 %	S ppm	H_2O %
Sulfur adsoption								
lean	6	470	0	0	100	10	30	10
rich	0	470	6	2	50	10	30	10
Sulfur desoption	0	0	0.13	0.09	0	15	0	10
NO_X storage measurement								
lean	6	470	0	0	100	10	0	10
rich	0	470	6	2	50	10	0	10

Table 3
Compositon of the solid after column separation

Elemint	Average measured weight (%)	Mol ratio
Ba	7.91	0.7
Ti	3.92	1.0
C	34.4	35.0

Table 4
Ba/Ti composition on Al_2O_3 primary particles observed in EDX analysis

area	Al wt%	Ti wt%	Ba wt%
1	90.4	5.8	3.8
2	85.4	7.1	7.3

Table 5
Amount and ratio to inlet sulfur of desorbed sulfur during sulfur desorption

Sulfur desorption temperature (°C)	Desorption sulfur amount and the ratio			
	BaTi-B		Ba-B	
	S_d (mmol/L)	R_d (%)	S_d (mmol/L)	R_d (%)
600	22.7	47.6	7.2	15.2
650	26.9	56.6	16.2	34.1

S_d: desorbed sulfur amount, R_d: the ratio of desorbed sulfur to inlet one

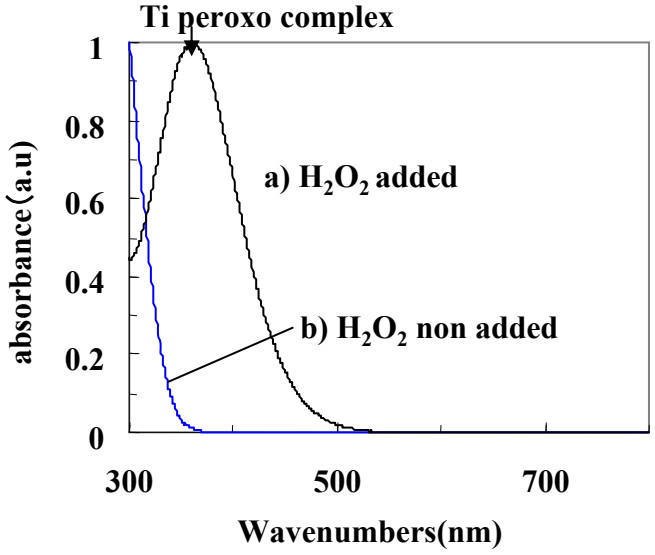

Fig. 1. UV-vis spectra of Ba-Ti precursor solutions.

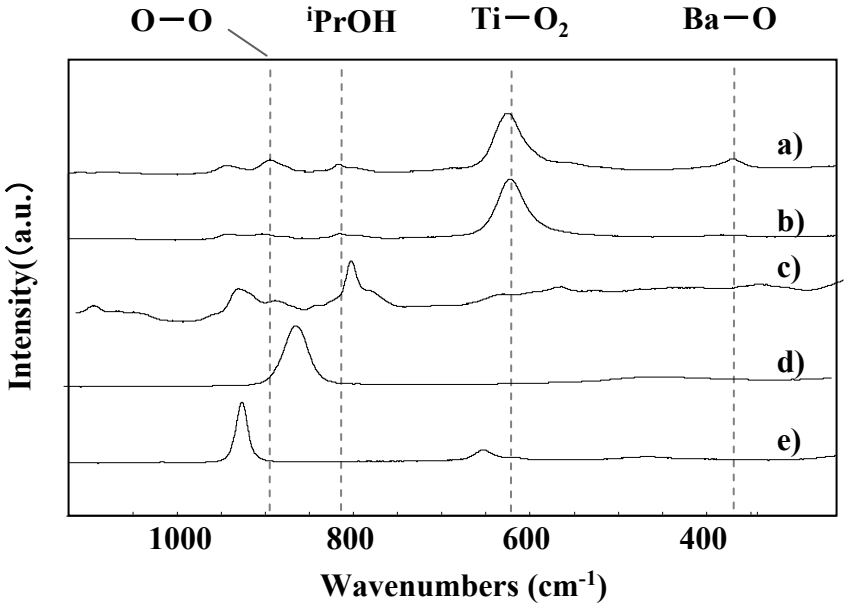

Fig. 2. Raman Spectra of the precursor solutions; a)BaTi precursor solution ($Ba(CH_3COO)_2$ + Ti citric acid + H_2O_2), b)Ti citric acid + H_2O_2 , c)Ti citric acid, d) H_2O_2 and e) $Ba(CH_3COO)_2$.

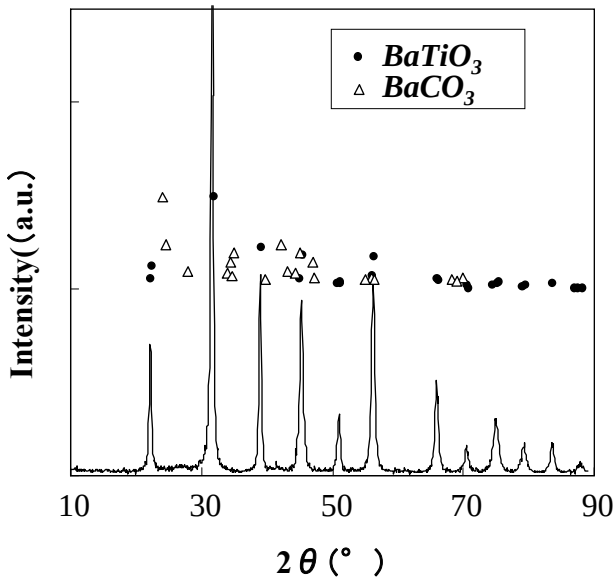

Fig. 3. XRD patterns of Ba-Ti composite oxides obtained after calcination of the precursor solutions at 650°C for 5h.

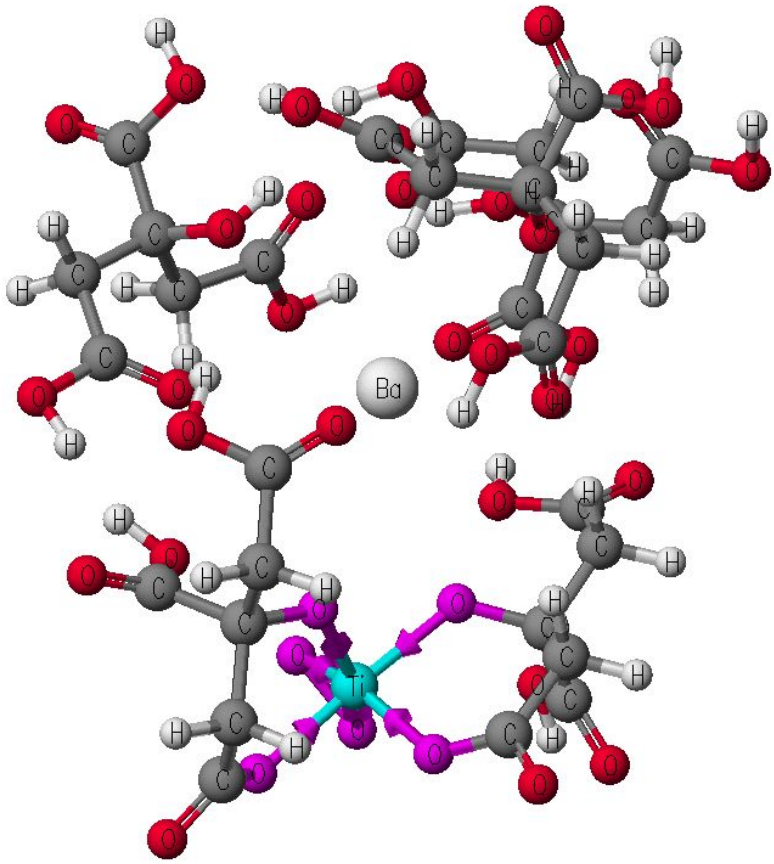

Fig. 4. Estimated structure of the Ba-Ti precursor complex.

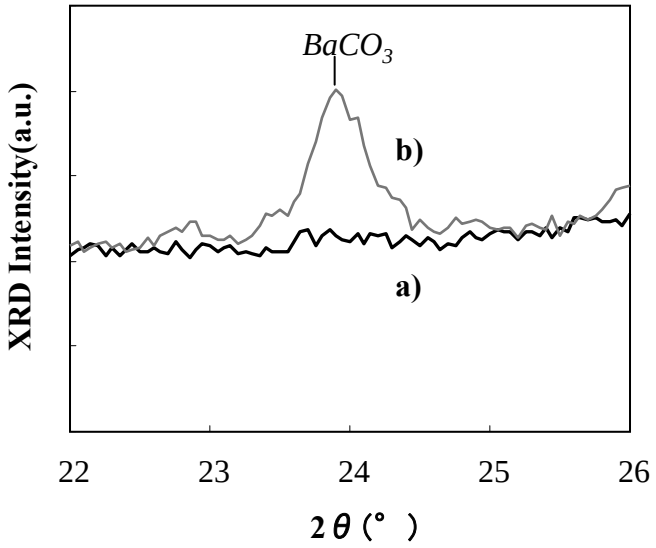

Fig.5. XRD patterns of fresh catalysts; a) BaTi-A and b) Ba-A.

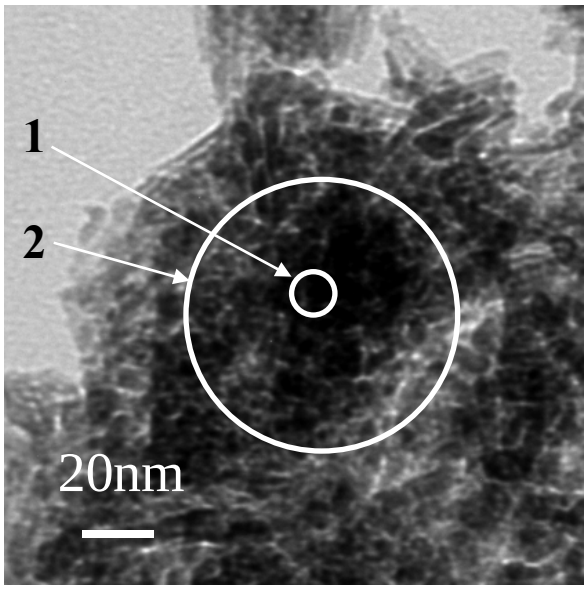

Fig. 6. FE-TEM micrograph of BaTi-A catalyst.

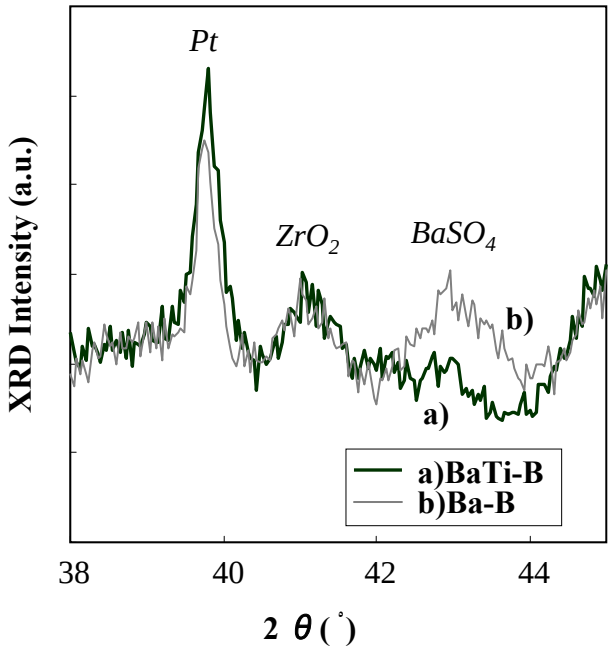

Fig. 7. XRD patterns of catalysts after sulfur aging; a)BaTi-B and b)Ba-B.

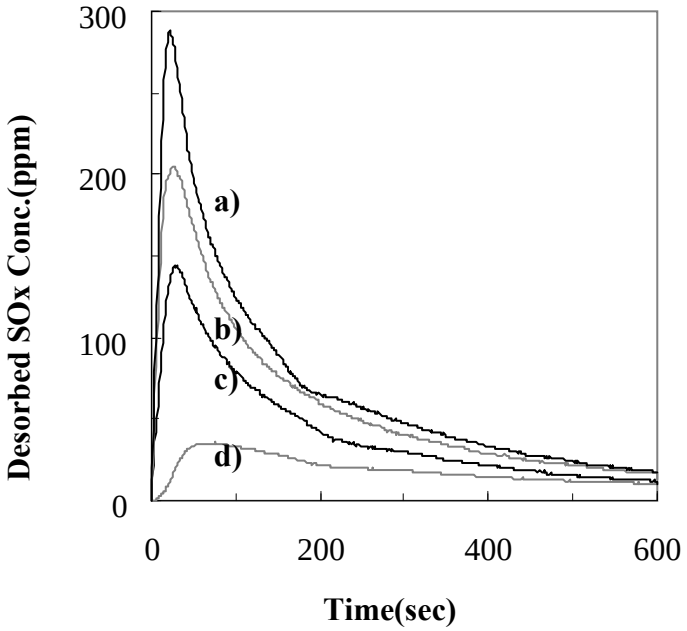

Fig. 8. Sulfur desorption profiles during SO_X regeneration from NSR catalysts; a) BaTi-B at 650 ˚C, b) BaTi-B at 600 ˚C, c) Ba-B at 650 ˚C and d) Ba-B at 600 ˚C.

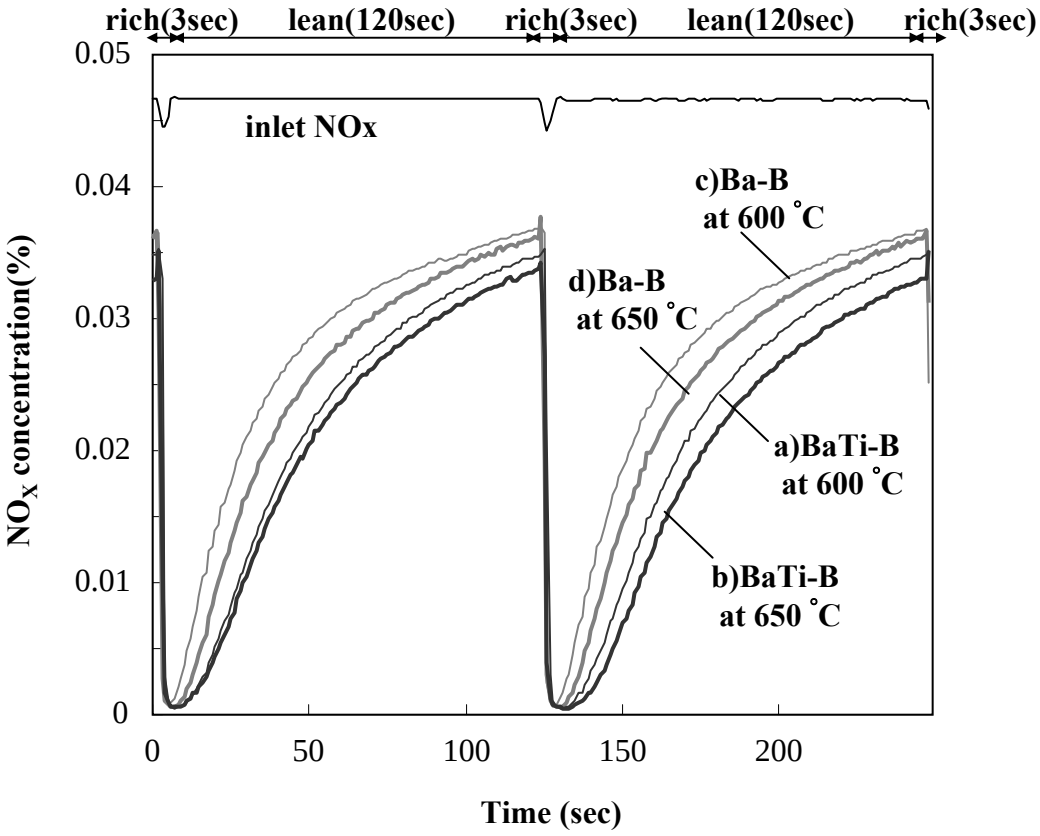

Fig. 9. NO_X concentration profiles at 400˚C during lean/rich cycle test over BaTi-B and Ba-B after the sulfur desorption procedure at 600 and 650˚C.

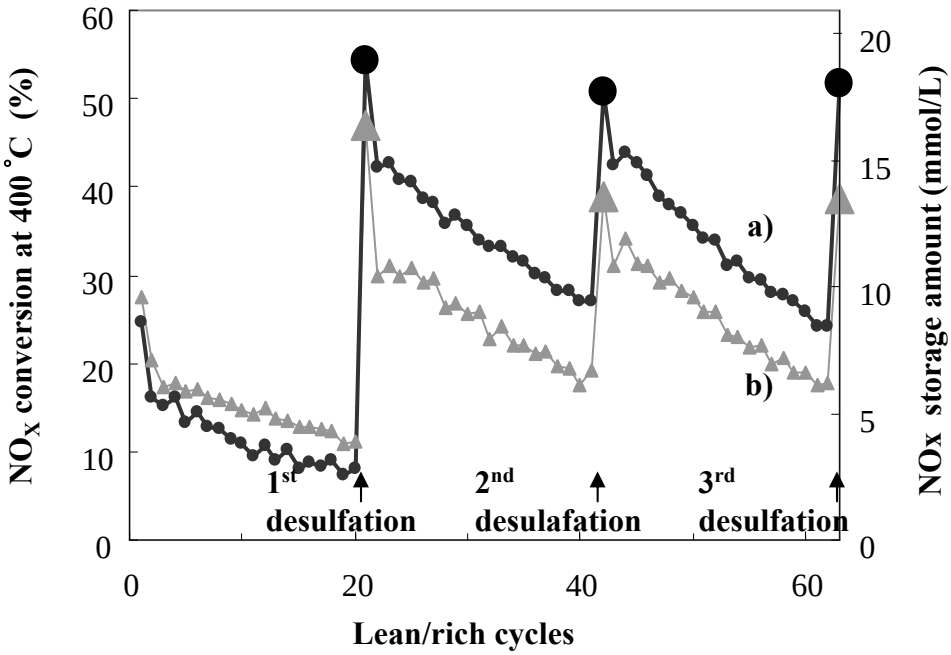

Fig. 10. NO_X conversion change at 400˚C during repetitive procedures (20 lean/rich cycles at 400˚C) and desorption (rich at 650˚C) over a) BaTi-B and b) Ba-B catalysts.

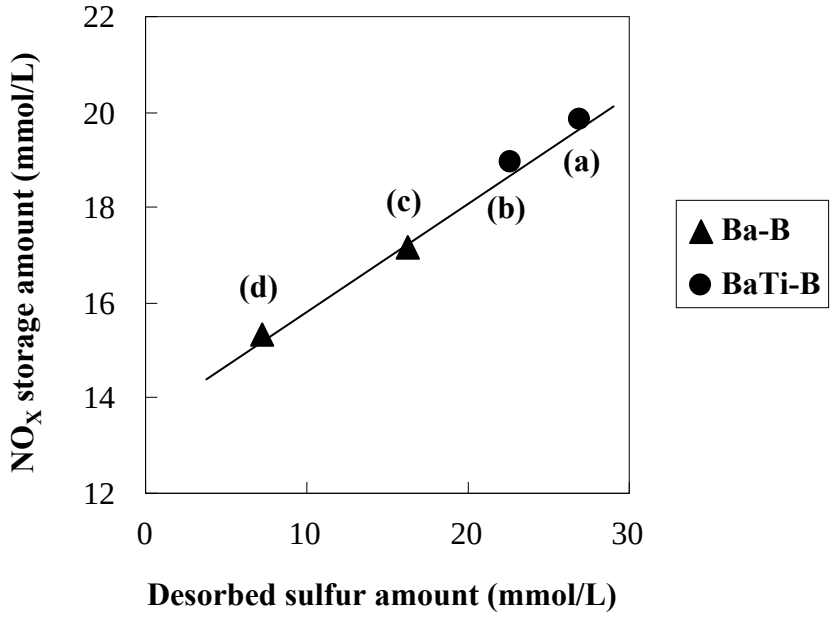

Fig. 11. The relationship between desorbed sulfur and NO_X storage amounts after sulfur regeneration at 600˚C or 650˚C; a) BaTi-B at 650˚C, b) BaTi-B at 600 ˚C, c) Ba-B at 650˚C and d) Ba-B at 600˚C.